Fast volumetric fluorescence lifetime imaging of multicellular systems using single-objective light-sheet microscopy

Valentin Dunsing-Eichenauer[1]#, Johan Hummert[2]#, Claire Chardès[1], Thomas Schönau[2], Léo Guignard[1], Rémi Galland[3], Gianluca Grenci[4], Max Tillmann[2], Felix Koberling[2], Corinna Nock[2], Jean-Baptiste Sibarita[3], Virgile Viasnoff[4], Ivan Michel Antolovic[5], Rainer Erdmann[2], Pierre-François Lenne[1]

1 Aix-Marseille Université & CNRS, IBDM—UMR7288 & Turing Centre for Living Systems, Marseille, France

2 PicoQuant GmbH, Rudower Chaussee 29, 12489 Berlin, Germany

3 Univ. Bordeaux, CNRS, Interdisciplinary Institute for Neuroscience, IINS, UMR 5297, F-33000 Bordeaux, France

4 Mechanobiology Institute, National University of Singapore, Singapore, Singapore

5 Pi Imaging Technology SA, EPFL Innovation Park, 1015 Lausanne, Switzerland

co-corresponding authors, co-first authors

ABSTRACT

Fluorescence lifetime imaging (FLIM) is widely used for functional and multiplexed bioimaging, but is limited in speed, volumetric sampling of multicellular specimen, and live cell compatibility. To overcome these limitations, we have combined single objective light-sheet microscopy with pulsed excitation and time-resolved detection on a SPAD array detector. We report excellent quantitative agreement with confocal FLIM at 10-100-fold shorter acquisition times, down to 100 ms per image. We demonstrate lifetime-based multiplexing in 3D and time-lapse FLIM of mechanosensitive tension probes on living embryonic organoids, providing a powerful tool for functional imaging of dynamic multicellular systems.

RESULTS AND DISCUSSION

Fluorescence lifetime imaging (FLIM) is a powerful technique to extend the information content of microscopy images beyond fluorescence intensity. Lifetime information can be used to multiplex different targets[1,2] or encode biophysically relevant parameters such as pH, temperature, membrane tension, and metabolic activity[3–6]. These sensing capabilities make FLIM especially suited for studies on living cells and multicellular systems. However, in its typical implementation in confocal laser scanning microscopes, applicability of FLIM to live samples is often limited by the trade-off between speed and phototoxicity. Light-sheet microscopy excels in exactly this trade-off, allowing for fast and gentle imaging.

Until recently, combining light-sheet microscopy and FLIM has been hampered by the availability of nanosecond time-resolved detectors for widefield microscopy. Previously employed detectors for light-sheet FLIM suffer from high dark currents in the case of

intensified or modulated cameras[7,8], from limited throughput in the case of multichannel plate-based detectors[9] or from limited fill factor and sensor size in the case of a novel SPAD-array[10,11]. A promising approach for high-speed FLIM of live samples is time-gating via fast Pockels cells[12,13], but this specialized technology is not readily available. Therefore, light-sheet FLIM has not yet realized its potential to enable faster lifetime imaging than state-of-the-art laser scanning microscopes. In addition, no quantitative comparison of light-sheet and confocal FLIM going beyond analysis of average lifetime has been performed. Here, we overcome these limitations by combining single-objective light-sheet microscopy (soSPIM) with a newly available SPAD-array detector. This configuration allows for the use of high numerical aperture (NA) objectives. The high collection efficiency is particularly beneficial for lifetime imaging and an added advantage over previous light-sheet FLIM implementations with multiple objectives, strongly limiting collection efficiency. We achieve FLIM at unprecedented speed in 3D, enabling multiplexing by lifetime and tension sensing in live organoids.

The soSPIM technology utilizes 45° mirrors embedded in microfabricated imaging devices to create a light-sheet perpendicular to the optical axis and collect the excited fluorescence through the same high NA objective that is used to illuminate the sample. Benefitting from this, we have previously demonstrated super-resolution STORM[14] and imaging fluorescence correlation spectroscopy using soSPIM[15]. Recently, we have also shown that soSPIM facilitates high content 3D imaging of a variety of organoid specimens[16], thanks to dedicated cell culture chips containing arrays of truncated pyramidal-shaped wells, each flanked with four micromirrors (JeWells).

To extend soSPIM to FLIM, we have equipped a soSPIM microscope with a newly developed pulsed laser and a state-of-the-art SPAD array detector. The laser is a prototype (PicoQuant GmbH) based on fiber amplification of mid-infrared laser diodes and frequency conversion. It delivers 60 ps pulses at 488 nm with an average power of up to 115 mW at 20 MHz repetition rate[17]. The detector is a 512x512 pixel gated SPAD-array (SPAD512^2, Pi Imaging Technology), enabling time-resolved imaging with a 6 ns global exposure gate that can be shifted with picosecond precision relative to the laser pulse. It has a peak detection efficiency of over 25% (quantum efficiency x fill factor) and a maximum total photon count rate of 6 GHz.

As a benchmark, we performed soSPIM and confocal FLIM measurements on the same samples, AF488 dye solution and fixed embryonic organoids (gastruloids) immunostained with E-cadherin-AF488. We evaluated soSPIM-FLIM performance in two light-sheet modalities: a digital scanned light-sheet generated by fast beam scanning along micromirrors and a static light-sheet created by a cylindrical lens. We acquired between 25 and 100 gate delays leading to FLIM frame exposure times between ca. 100 ms and 1 s (Fig. 1a), with 0.41 µm pixel size and a field-of-view of 210 µm. For confocal measurements, we used a conventional TCSPC system limited to ca. 4 MHz photon count rate and a state-of-the-art rapidFLIM system that supports photon count rates of up to 80 MHz[18] (Fig. 1a). As a metric for FLIM performance, we quantified the average and standard deviation of lifetime histograms and photon counts in the brightest pixels, for different acquisition times (Fig. 1c). For organoid measurements, only pixels within the organoid and above a global intensity threshold (Otsu) were considered in the comparison to exclude background pixels. We found excellent agreement between pixel lifetimes measured by confocal and soSPIM-FLIM (Fig. 1b, Fig. S1-3). However, soSPIM measurements provided a far more precise estimate within shorter acquisition times. Even in comparison to rapidFLIM, ca. 2x narrower lifetime histograms were achieved in 2x shorter acquisition time in scanning light-sheet mode. In

static mode, approximately 4x narrower histograms were achieved in 10x shorter acquisition time than in rapidFLIM. Correspondingly, approximately 1000 counts in the brightest pixel and similar histogram widths were achieved in 100 ms with static light-sheet, in 1.3 s with scanning light-sheet, and in 10.9 s with RapidFLIM (Fig. 1b). Strikingly, in comparison to rapidFLIM, high photon counts were generated with 70 and 300 times lower power densities for scanning and static soSPIM-FLIM respectively (Table S1).

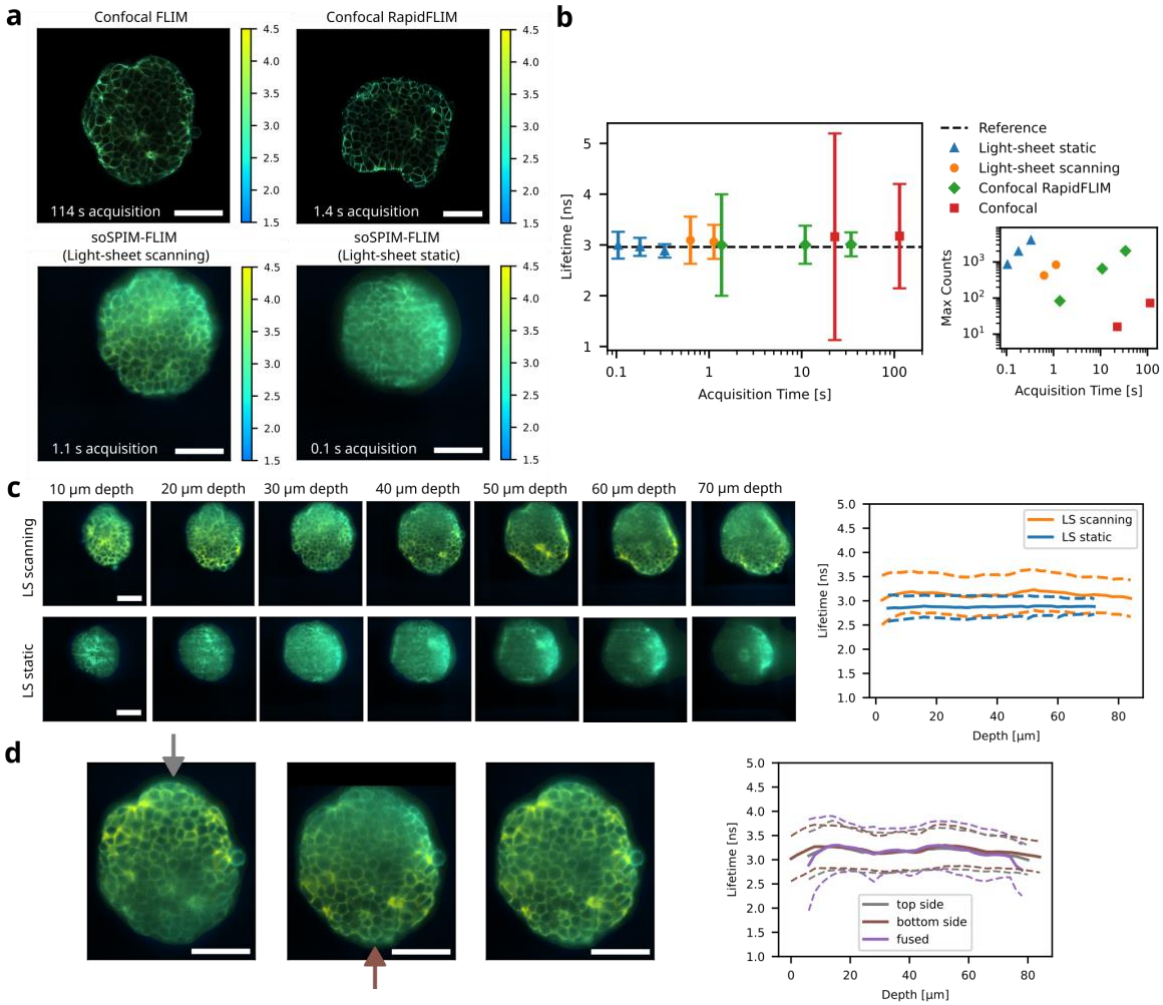

Figure 1 – Benchmarking of soSPIM-FLIM in 3D embryonic organoids.
(a) Exemplary FLIM images of fixed embryonic organoids stained with E-cadherin-AF488, acquired with a conventional or RapidFLIM confocal microscope (top row, scale bar is 50 µm) or soSPIM-FLIM in scanning or static light-sheet mode. Measurements were performed at 30-50 µm depth. Acquisition times are indicated. **(b)** Average and standard deviation of lifetime histograms obtained for the measurements shown in (a), pooled from all pixels within the organoid. For confocal data, an increasing number of frames were sampled from the same measurement. The reference is the intensity weighted average lifetime from sum fits of lower power confocal measurements (Fig. S3). The inset shows average maximum photon counts in the brightest pixels (excluding the top 0.1% of pixels) **(c)** soSPIM-FLIM images obtained in 3D acquisitions with scanning or static light-sheet with 1 s (scanning) or 0.1 s (static) exposure time per plane. 3D soSPIM-FLIM stacks were acquired over a range of 80 µm with 2 µm spacing. The graph on the right shows the average lifetime and standard deviation over the whole image as a function of imaging depth. **(d)** Dual-illumination soSPIM-FLIM images at 40 µm depth obtained from sequential 3D acquisition from opposing JeWell mirrors at the top or bottom of the image. Image stacks were registered and fused to obtain a final FLIM image with a more uniform image quality. Right: Average lifetime and standard deviation as a function of image depth for both illumination sides and the fused image.

To evaluate the dynamic range of soSPIM-FLIM, we analyzed the lifetime as a function of pixel count rate for different illumination powers. To account for saturation of the detector, i.e. incident photons that are missed per single-bit exposure after detection of a photon, we applied a pile-up correction[19]. The scanning light-sheet is much more prone to pile-up due to the limited scanning frequency of the beam, causing local saturation of gates with the highest photon count rate in pixels that are illuminated during the passage of the beam. To account for this, we employed an adapted pile-up correction to the scanning light-sheet data (see Methods and SI for details). Nonetheless, the measurement speed and dynamic range of scanning light-sheet remain limited by detector saturation. Static light-sheet achieves approximately 10x faster acquisition at comparable count rates than scanning light-sheet (Fig. 1, Table S1).

The fast speed of soSPIM-FLIM makes it ideally suited for 3D acquisitions. To demonstrate this, we performed 3D FLIM measurements in organoids across an 80 µm range, with one image plane every 2 µm, illuminated for 180 ms in static mode and 1 s in scanning mode (Fig. 1c). While the average pixel lifetime is constant across z, we observe a ca. 10% discrepancy between lifetimes determined from static and scanning light-sheet measurements. This is likely explained by residual pile-up in scanning light-sheet in high intensity pixels, also visible as yellow areas in Fig. 1c. Besides much faster speed, soSPIM-FLIM benefitted from less photon loss at deeper z planes compared to confocal FLIM, which showed darker regions in the inside of organoids at 50 µm depth (Fig. S2). On the contrary, soSPIM-FLIM showed a lower optical sectioning and a strong degradation of image quality and photon counts in the more distant part of the aggregate with respect to the illumination side due to the gaussian light-sheet profile (Fig. 1c,d). In light-sheet microscopy, this is commonly circumvented by illuminating the specimen from multiple sides[20,21]. Benefitting from the JeWell architecture, which can provide up to four illuminated sides, soSPIM-FLIM can be readily adapted to larger specimens. To demonstrate this, we performed sequential dual-illumination soSPIM-FLIM from two opposing sides of the JeWell mirrors and fused the acquired image stacks to a final, uniform 3D FLIM image stack (Fig. 1d).

A powerful application of FLIM is lifetime unmixing, i.e. to discriminate spectrally overlapping fluorophores by their fluorescence lifetime, providing an additional contrast for multi-color imaging[1,22]. In light-sheet microscopy, lifetime-based multiplexing could allow simultaneous imaging of targets that would otherwise be imaged sequentially and simplify microscope setups that require multiple laser lines and cameras. To test lifetime unmixing, we stained live embryonic organoids expressing nuclear H2B-GFP fusion protein with Flipper-TR, a membrane tension sensor that stains the plasma membrane of cells (Fig. 2a). We performed 3D soSPIM-FLIM in scanning mode with 1 s acquisition time per plane. Lifetime images obtained with soSPIM showed a clear contrast between nuclei and membrane pixels (Fig. 2b). To extract the characteristic lifetimes for both species, we selected two populations in the phasor plot[23,24] (Fig. 2a). We then mapped selected points back to the original image, providing masks that showed clear correspondence to either nuclei or membrane pixels. Fitting a double-exponential fit model to the summed decays provided a short and long lifetime component for each species. We performed this analysis in 3 organoids at 3 different depths (10 µm, 30 µm, 50 µm) and obtained robust lifetime estimates of 2.1±0.2 ns, 5.4±0.9 ns for species one (i.e. GFP) and 1.0±0.2 ns, 4.8±0.2 ns for species two (i.e. Flipper-TR) (Fig. 2b). Notably, these values were in good agreement with confocal lifetimes determined from FLIM images acquired for 4 min on the same organoids by manual ROI selection and two-component fitting (Fig. S8), even for sampling with only 50 gate delays (Fig. 2b). The slightly lower lifetimes measured for Flipper-TR with soSPIM-FLIM are likely a consequence of the lower excitation wavelength (i.e. 488 nm) compared to confocal FLIM (i.e. 510 nm), as recently shown[25]. Finally, we fitted a superposition model of both lifetime patterns to each

pixel, providing amplitudes that we then used to calculate unmixed intensity images (Fig. 2c). With this pipeline, we could well separate nuclei and membranes, i.e. GFP and Flipper-TR signal, which is only separated by 1 ns in the amplitude-weighted average lifetime (see SI). Lifetime unmixing worked reliably in different z planes across 70 µm depth in multiple organoids (Fig. 2d). We hereby benefitted from the multi-position imaging capabilities of soSPIM[16], which allowed us to perform soSPIM-FLIM on multiple organoids located in the same JeWells chip (Fig. 2d), without requiring time-consuming re-alignment or repositioning of the beam for each organoid[16].

The speed and gentleness of soSPIM-FLIM make it an ideal tool for time-lapse FLIM on sensitive, dynamics specimens, which is strongly limited with confocal FLIM due to requirements for either high excitation powers or long acquisition times to achieve sufficient photon counts. As a proof-of-concept, we performed 3D time-lapse soSPIM-FLIM on live embryonic organoids stained with Flipper-TR, a mechanosensitive membrane tension sensor recently applied to *in vivo* specimens[26]. Due to the limited photon budget in confocal FLIM, its lifetime is usually determined globally across many cells acquired in one plane for several minutes. With soSPIM-FLIM, we could quantify Flipper-TR lifetime over time in individual, fastly rearranging cells or even individual junctions from, on average, 90 000 photons detected per cell (ca. 15 000 per junction) in 1 s acquisition time per 2D plane of a 3D time-lapse acquisition across 60 µm and over a course of 60 min. (Fig. 2e, Fig. S9). We observed a decrease in Flipper-TR lifetime in two cells over the observation time of 1 h, which is in line with a decrease in membrane tension[27]. The decrease in lifetime is not correlated with changes in count rate, showing that this is not an artifact of pile-up or reduced counts due to photobleaching (Fig. 2f).

The 3D tension imaging shows that the combination of single objective light-sheet microscopy and fluorescence lifetime imaging opens up new possibilities for functional imaging on living samples. Light-sheet FLIM enables gentler and faster lifetime imaging with robust results in excellent agreement with confocal FLIM. Even in the digital scanned light-sheet modality, which is limited by detector pile-up at currently available scan rates, we showed lifetime multiplexed imaging in 3D. Our benchmark demonstrates that static light-sheet illumination has clear advantages when combined with the time-gated detector architecture employed here.

While this shows that additional considerations regarding the interplay between illumination and sensor architecture are required, the simplicity of adding pulsed excitation and a time-resolved camera to a light-sheet microscope will enable FLIM in new contexts in the future. In conjunction with our recently presented high-throughput 3D imaging pipeline[16], soSPIM-FLIM can be automatized to achieve high-content 3D FLIM imaging, providing a throughput of about 50 organoids per hour. Together with, for instance, metabolic imaging and the increasing number of organoid models, this could become a key tool to better understand human physiology in health and disease.

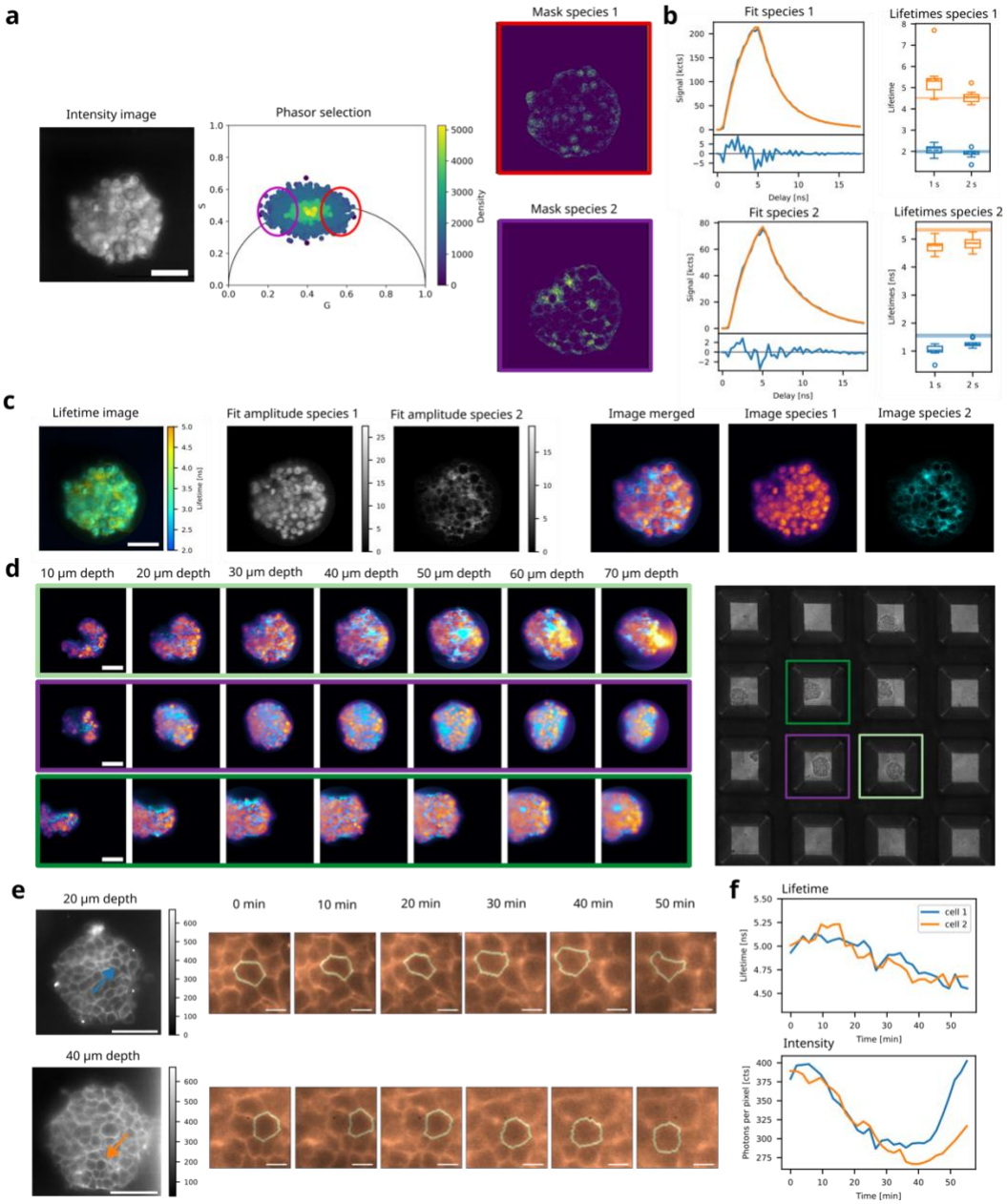

Figure 2 – Application of soSPIM-FLIM for lifetime unmixing and live time-lapse 3D FLIM.
(a) Pipeline for generation of lifetime patterns for organoids expressing H2B-GFP and additionally stained with Flipper-TR (grayscale image). To identify the two species, soSPIM data were transformed into phasor space and points selected using elliptic cursors drawn around the extremities of the point cloud. Backmapping selected points to the image generates two masks. **(b)** Two-component fitting was performed to extract characteristic lifetimes for the two species. Box plots show lifetimes obtained in three different organoids at three different z planes from measurements with acquisition times of 1 and 2 s in scanning mode. Horizontal lines indicate reference lifetime values extracted from confocal FLIM performed on the same samples (Fig. S8). **(c)** Lifetime unmixing for H2B-GFP/Flipper-TR organoids using lifetime patterns described in (b). Pixel-wise fitting with the determined lifetime patterns results in species amplitudes, which are used to generate unmixed intensity images (right), showing successful decomposition into nuclei and membrane signal. **(d)** Composite images obtained by unmixing of slices from 3D soSPIM-FLIM data on the samples described in (a,b), imaged across 70 µm with 2 µm spacing and 1 s acquisition time per plane. Shown are three different organoids from a multi-position acquisition on one JeWell chip (brightfield image of wells shown on the right). **(e)** 3D time-lapse soSPIM-FLIM imaging of live organoids stained with Flipper-TR was performed over ca. 60 min in scanning mode, with 2 µm spacing across 60 µm z-range. Individual cells (blue and orange arrow for cells at 20 µm and 40 µm depth) were segmented and tracked semi-automatically (white mask). **(f)** The Flipper-TR lifetimes of the tracked cells are determined from the average decay of all segmented membrane pixels. The plot shows the long lifetime from a two component fit with the short lifetime fixed (see methods). The analysis was restricted to a single 2D plane per cell. Scale bars are 50 µm in the left image and 10 µm in the cropped images.

MATERIALS AND METHODS

Microscope setups

soSPIM-FLIM microscope

Light-sheet imaging was performed on a custom-made soSPIM microscope built around a Zeiss Axiovert 200 microscope body (Carl Zeiss) following the previously published design[14]. It consists of a custom laser scanning unit, dedicated microfabricated devices[16] containing an array of truncated pyramidal-shaped microwells flanked with 45° mirrors (JeWells), and a soSPIM acquisition module operating in MetaMorph (Molecular Devices). The microscope is equipped with an LED lamp (CooLED, Andover) for brightfield imaging, continuous-wave excitation lasers at 488, 514 and 561 nm and an sCMOS camera (Hamamatsu ORCA Flash 4.0 V3). The sample is illuminated and fluorescence is detected through a 40x 1.2 NA Plan Apochromat water-immersion objective (Carl Zeiss). The light-sheet was generated by either scanning the laser beam laterally along the JeWell mirrors or by inserting a cylindrical lens (f=150 mm, Thorlabs) into the optical path and aligning it according to the JeWell mirrors axis[14,15]. 3D imaging is achieved by moving the beam perpendicular to the mirror axis through a pair of galvanometric mirrors (Pangolin SCANMAX 506 actuators) while translating the objective axially using a piezo-driven focus controller (Physik Instrumente). The resulting displacement of the light-sheet waist is compensated by shifting it using an electrical tunable lens (Custom EL-30-10, Optotune). The light-sheet position (axial position and waist) is synchronized with the focal plane of the objective thanks to the soSPIM acquisition module, which ensures optimal 3D sectioning. The dimensions of the light-sheet were controlled by adjusting the laser beam diameter using a tunable diaphragm placed after the fiber output of the coupled excitation lasers. The resulting dimensions for scanning and static light-sheet were ca. 1.5 µm/ 1.9 µm waist and ca. 50 µm/ 80 µm Rayleigh length. The width of the static light-sheet was ca 110 µm.

For FLIM detection, a 512x512 pixel SPAD array detector (SPAD512[2], Pi Imaging Technology) was mounted on the second port of the microscope. The image plane of the detector was aligned with the sCMOS camera and centered on the same field of view. The effective field-of-view of the SPAD array is 210x210 µm^2 with a pixel size of 410 nm. For FLIM excitation, a high power pulsed 488 nm laser prototype[17] (PicoQuant GmbH) was fiber coupled into the optical path. Time gating of the SPAD array detector was triggered by the laser via a NIM to TTL converter (TMF400, PicoQuant GmbH). For 3D FLIM imaging, image acquisition on the SPAD array was synchronized with soSPIM illumination using a TTL trigger signal. To achieve dual-illumination imaging from two sides, two opposing mirrors of a JeWell were illuminated sequentially. The sample was shifted in between to fit it into the field of view of the SPAD array detector. For each side, the waist of the light-sheet was positioned at a distance of about one quarter of the specimen's thickness from the reflecting mirror. To image multiple organoids in different positions , the previously described tools for JeWell chip preview and positioning of individual JeWells were employed using bright field imaging[16]. For live imaging, the JeWell chip was placed into an incubation chamber (Okolab), which was mounted on top of the microscope stage, heated up to 37°C and provided with 5% CO_2 and 85% humidity.

Confocal FLIM microscope

FLIM measurements were performed on a Zeiss LSM880 system (Carl Zeiss) equipped with a time-resolved LSM upgrade (PicoQuant GmbH) using a Plan-Apochromat 40x, 1.2 NA water immersion objective. Images of 512x512 pixels per frame were acquired after excitation with a 510 nm pulsed laser diode operating at 20 MHz repetition rate. Fluorescence was split using a 560 nm dichroic mirror and detected by two PMA Hybrid-40 detectors (PicoQuant) after

passing 550/49 nm and 600/50 nm bandpass filters, respectively. The pinhole was set to 1 airy unit. In each measurement, images were accumulated over a time period of 2 min, with a pixel dwell time of 1.23 µs and frame time of 0.6 s.

Rapid FLIM confocal microscope

Rapid FLIM Measurements were performed on a MicroTime 200 confocal microscope (PicoQuant GmbH) equipped with a LDH-D-C-485 picosecond excitation laser, a FLIMBee beam scanner, a PMA Hybrid-40 detector, and a MultiHarp 150 TCSPC unit[28] (all PicoQuant GmbH). RapidFLIM images of fixed organoids stained with E-cadherin-AF488 were acquired with a 60x 1.2 NA water immersion objective (UPLSAPO60XW, Olympus), with 485nm pulsed excitation at a 40 MHz laser repetition rate with 512x512 pixels, 500 nm pixel size, and a dwell time of 1.3 µs.

Data acquisition

FLIM data acquisition was performed with the Pi Imaging software in streaming mode, controlled by self-written Python scripts. The light-sheet microscope was controlled via MetaMorph (Molecular Devices). Confocal microscopes were controlled with ZEN (Carl Zeiss) and SymPhoTime64 (PicoQuant) in the case of the LSM880 and with SymPhoTime64 in the case of the MicroTime 200.

Data Analysis

Instrument response function

The combined instrument response function (IRF) of the SPAD-array and the laser was characterized by detecting reflected laser light from a mirror placed on the sample holder. The measured IRF is parametrized with an approximated function, given by integration of a Gaussian laser IRF with an infinitely sharp gate edge:

$$IRF(t) = \sqrt{\frac{\pi}{2}}\sigma \left[\mathrm{erf}\left(\frac{t - t_0 + w}{\sqrt{2}\sigma}\right) - \mathrm{erf}\left(\frac{t - t_0}{\sqrt{2}\sigma}\right)\right]$$

with the gate width w, the width of the laser IRF σ, and the gate delay offset t_0 as free parameters. With this IRF model the sigma parameter compensates for the finite edge steepness of the SPAD-array gating function, and is a measure for the combined edge steepness given by the laser pulse width and the detector gating function. By parametrizing the IRF, relative delays between the IRF and light-sheet measurements can be compensated and the high demands for experimental IRF data quality are relaxed (Fig. S10).

Background and pile-up correction

To limit the impact of dark counts, background measurements (Fig. S10) were taken daily with the same settings as the fluorescence measurements and subtracted from measured data. To account for detector saturation, we employed an adapted pile-up correction[29]. The corrected photon number in 8-bit images is calculated from the measured photon number as:

$$N_{corr} = -ln\,(1 - N * F/255) * 255/F$$

with $F=1$ for static light-sheet measurements and $F=3.5$ for scanning light-sheet measurements. Pile-up correction was applied after background correction. A detailed discussion of pile-up correction can be found in the SI.

Phasor analysis

Phasor plots were generated using a discretized phasor transformation[24]. From the detected lifetime decay $N_{m,ij}$ in each pixel ($N_{m,ij}$: photon count in gate delay m in pixel ij), the phasor coordinates were calculated as follows:

$$G_{ij} = \frac{\sum_{m=0}^{k-1} N_{m,ij} cos\left(\omega\left(m+\frac{1}{2}\right)\Delta T\right)}{\sum_{m=0}^{k-1} N_{m,ij}},$$

$$S_{ij} = \frac{\sum_{m=0}^{k-1} N_{m,ij} sin\left(\omega\left(m+\frac{1}{2}\right)\Delta T\right)}{\sum_{m=0}^{k-1} N_{m,ij}},$$

where $\omega = 2\pi/T$, with the total detection time T, the gate width Δt and k the number of gate delays. To account for the IRF, the total phasor and the phasor of the IRF were calculated in complex space and the IRF phasor divided from the total phasor in each pixel. Afterwards, the real and imaginary parts G_{ij} and S_{ij} were determined.

Fitting

Time-gated FLIM signals are fitted with an approximate model function. This is based on an analytic approximation function for the convolution of a Gaussian pulse with an exponential decay, according to[30]:

$$f(t) = \frac{1}{2}\exp\left(\frac{\sigma^2}{2\tau^2}\right)\left(1 - \mathrm{erf}\left(\frac{\sigma}{\sqrt{2}\tau} - \frac{t}{\sqrt{2}\sigma}\right)\right)\exp\left(-\frac{t}{\tau}\right),$$

where σ is the width of the gaussian pulse and τ is the monoexponential decay time. The model function for decays obtained by time-gated detection is then obtained by integrating the decay function with infinitely sharp gate edges, analogous to the model function for the IRF:

$$f_{Gated}(t) = A\frac{\tau}{2}\exp\left(\frac{\sigma^2}{2\tau^2}\right)\left[\left(\mathrm{erf}\left(\frac{\sigma}{\sqrt{2}\tau} - \frac{t-t_0+w}{\sqrt{2}\sigma}\right) - 1\right)\exp\left(-\frac{t-t_0+w}{\tau}\right) + \exp\left(-\frac{\sigma^2}{2\tau^2}\right)\mathrm{erf}\left(\frac{t-t_0+w}{\sqrt{2}\sigma}\right)\right]$$
$$- A\frac{\tau}{2}\exp\left(\frac{\sigma^2}{2\tau^2}\right)\left[\left(\mathrm{erf}\left(\frac{\sigma}{\sqrt{2}\tau} - \frac{t-t_0}{\sqrt{2}\sigma}\right) - 1\right)\exp\left(-\frac{t-t_0}{\tau}\right) + \exp\left(-\frac{\sigma^2}{2\tau^2}\right)\mathrm{erf}\left(\frac{t-t_0}{\sqrt{2}\sigma}\right)\right],$$

where A is the decay amplitude, t_0 can express a time offset between the gate delays and the laser pulse and w is the width of the approximated gate. The use of this analytic model function without explicit convolutions not only speeds up pixel-wise fitting, but also simplifies the use of the parametrized IRF and thus the compensation of IRF variations across the detector area (see SI). The IRF parameters σ and w were held fixed at the extracted pixel values from the IRF measurement for all fits. Maximum likelihood estimation of model parameters from experimental decay signals was performed with the L-BFGS-B implementation within the scipy optimize package.

Pattern Matching

To decompose FLIM images on organoids containing two fluorophore species, i.e. GFP and Flipper-TR, phasor plots of FLIM images were generated in three different z planes (i.e. at 10, 30 and 50 µm depth) for three different organoids. In each phasor plot, two elliptic cursors were drawn around the extremities of the point cloud and selected points mapped back to the image to define pixel masks for individual fluorophore populations. Lifetime decays were then summed across all corresponding pixels and a double-exponential decay model fitted to the overall decay for each species. Averaging over all organoids and z depths, this procedure yielded two characteristic lifetimes and respective amplitudes for each species, defining their lifetime patterns. Next, a superposition model, defined as the sum of the two lifetime patterns (i.e. two double exponential decay functions, each with fixed decay times and amplitudes) was fitted pixel-wise to the lifetime decay in each pixel of the 3D FLIM stack with species

amplitudes as free fit parameters. Final intensity images for each species were generated by weighing the total pixel intensity in the original image with the determined species amplitudes. Before intensity weighting, the amplitudes were smoothed with a gaussian kernel (sigma=1 pixel) to reduce pixel-to-pixel variations.

Dual-illumination registration and fusion

Image stacks acquired from two opposite illumination sides were first registered in 3D using the Blockmatching algorithm[31] based on a 3D translation. In the registered image stacks, aggregates were segmented in a maximum intensity projection after Gaussian blurring with a sigma of 10 pixels, mean thresholding and dilation of the obtained mask with disk of radius 10. A bounding box surrounding the union of the two segmentation masks was then calculated and fusion weights $w_{1,2}$ defined using a sigmoid function,

$$w_{1,2}(x) = \frac{1}{e^{\pm\frac{x-l/2}{l/8}}+1},$$

centered around the mid-line of the bounding box, where l is the width of the bounding box, x the spatial coordinate along the light propagation axis. Image and lifetime stacks were then fused using a weighted sum[32,33],

$$I(x,y,z) = \frac{w_1(x)I_1(x,y,z)+w_2(x)I_2(x,y,z)}{w_1(x)+w_2(x)},$$
$$\tau(x,y,z) = \frac{w_1(x)\tau_1(x,y,z)+w_2(x)\tau_2(x,y,z)}{w_1(x)+w_2(x)},$$

where $I_{1,2}$ and $\tau_{1,2}$ are the intensity and lifetime stacks acquired from each illumination side and (x,y,z) denote the spatial coordinate of each image voxel.

Cell segmentation and Flipper-TR time-lapse analysis

For individual cell lifetime analysis of 3D time-lapse Flipper-TR data, cells of interest were selected and, for each time point and cell, the image containing the cell at its central z-position extracted from the z-stack. Cell membranes were segmented in these images in 2D, using the Tissue Analyzer plugin[34] in Fiji[35]. Label images containing a separate label for each segmented junction were manually curated in Napari[36] and junctions belonging to the same cell pooled to obtain segmentation masks for each time point. Subsequently, cells masks were manually annotated in time. Finally, masks were dilated with a disk kernel of radius of one pixel to account for the width of the cell outlines in the images. Decays were summed over all pixels belonging to the same cell and fitted with a two-component decay model. The short lifetime was first left as a free fit parameter and then fixed to its time-averaged value for the final fitting iteration (Fig. S9).

Confocal FLIM

All confocal FLIM data were analyzed using the SymPhoTime64 software (PicoQuant GmbH, Berlin, Germany). For pixelwise single exponent estimation (Ecad-AF488) the fast lifetime algorithm is used, corresponding to center of mass analysis. For reference lifetimes of single fluorophore data, bi-exponential re-convolution fitting of sum signals at moderate intensity is performed (Fig. S3). For reference lifetimes of dual-labelled samples, decay patterns were generated from manually selected ROIs (Fig. S8) of nuclei and membranes. Sum decays of the ROIs were fitted with a bi-exponential re-convolution fit to obtain the reference lifetimes given in Fig. 2.

Sample preparation

Solution measurements

Alexa Fluor 488 (AF-488) NHS Ester (ThermoFisher Scientific) was dissolved in PBS at 200nM and pipetted onto the soSPIM chip for imaging.

Gastruloid culture, staining and mounting

A complete description of the culture conditions and the protocol for making gastruloids is presented in Baillie-Johnson et al., 2015[37]. In the experiments presented here, gastruloids were generated from E14Tg2a.4 or H2B-GFP mouse embryonic stem cells (mESC) (MMRRC, University of California Davis, US) using an initial cell number of 100, and cultured according to the modified protocol described in Hashmi et al., 2022[38]. After 2 days of culture, gastruloids were incubated for 1 h in culture medium supplemented with 1 µM Flipper-TR and manually transferred to JeWell chips with 120 or 170 µm well size (top opening). E14 gastruloids were fixed using 4% paraformaldehyde and immunostained for E-cadherin using rat primary antibody and anti-rat-AF-488 secondary antibody, following published protocols[38]. JeWell culture chips were rinsed with 96% ethanol, passivated with 0.2% lipidure solution and rinsed in PBS after evaporation. To remove air bubbles, chips were evacuated in a vacuum chamber for 1 h. Afterwards, chips were sterilized under UV illumination for 30 min and medium was exchanged to cell culture medium using multiple washes. Live or fixed gastruloids were mounted manually by pipetting under the occular (source) just before imaging. For RapidFLIM measurements, fixed gastruloids were placed in a 35mm glass-bottom dish (#1.5, MatTek Corp., Ashland, MA)

AUTHOR INFORMATION

Corresponding Authors
Valentin Dunsing-Eichenauer, valentin.dunsing@univ-amu.fr
Johan Hummert, hummert@picoquant.com

Author Contributions
V.D.-E., J.H. conceived the project idea, coordinated the project, performed all experiments, wrote the analysis code, analyzed and visualized all data, co-wrote the manuscript. V.D.-E., J.H. and C.C. aligned the optical setup. V.D., J.H. and P.-F.L. discussed the results. T.S. and C.N. designed and built the 488 nm laser prototype. L.G. provided software. R.G. provided assistance with the optical setup. G.G. conceived and fabricated the JeWell chips. M.T. assisted with data analysis. R.G., G.G., J.-B.S. and V.V. developed the soSPIM technology. I.M.A. developed the SPAD array detector. R.E. and P.-F.L. provided funding and equipment. All authors co-edited the manuscript.

ACKNOWLEDGEMENT

We thank Agathe Rostan (IBDM Marseille) for help with sample preparation, Frank Schnorrer (IBDM Marseille) for access to the confocal FLIM system. We thank Daniel Sapede and Brice Detailleur from the IBDM imaging facility for technical assistance. V.D. acknowledges support by an HFSP long-term postdoctoral fellowship (HFSP LT0058/2022-L). This work is supported by the French National Research Agency (“Adgastrulo” project ANR-19-CE13-0022) and the Fondation de la Recherche Médicale (to P.-F.L. EQU202003010407). We also acknowledge the France-Bioimaging Infrastructure (ANR-10-INBS-04). The picosecond pulsed laser at 488 nm was developed as part of LIVE2QMIC project funded by the BMBF in the program "Photonics Research Germany" (BMBF 13N15953).

CONFLICT OF INTEREST

J.H., T.S., M.T., F.K., and C.N. are employed at PicoQuant GmbH, R.E. is the CEO and co-founder of PicoQuant GmbH, I.-M.A. is the CEO and co-founder of Pi Imaging Technology.

REFERENCES

1. Niehörster, T. *et al.* Multi-target spectrally resolved fluorescence lifetime imaging microscopy. *Nat. Methods* **13**, 257–262 (2016).

2. Frei, M. S. *et al.* Engineered HaloTag variants for fluorescence lifetime multiplexing. *Nat. Methods 2021 191* **19**, 65–70 (2021).

3. Colom, A. *et al.* A fluorescent membrane tension probe. *Nat. Chem. 2018 1011* **10**, 1118–1125 (2018).

4. Barroso, M., Monaghan, M. G., Niesner, R. & Dmitriev, R. I. Probing organoid metabolism using fluorescence lifetime imaging microscopy (FLIM): The next frontier of drug discovery and disease understanding. *Adv. Drug Deliv. Rev.* **201**, 115081 (2023).

5. Okabe, K. *et al.* Intracellular temperature mapping with a fluorescent polymeric thermometer and fluorescence lifetime imaging microscopy. *Nat. Commun. 2012 31* **3**, 1–9 (2012).

6. Shimolina, L. *et al.* Fluorescence lifetime-based pH mapping of tumors in vivo using genetically encoded sensor SypHerRed. *Biophys. J.* **121**, 1156–1165 (2022).

7. Liu, X. *et al.* Fast fluorescence lifetime imaging techniques: A review on challenge and development. *J. Innov. Opt. Health Sci.* **12**, 12 (2019).

8. Mitchell, C. A. *et al.* Functional in vivo imaging using fluorescence lifetime light-sheet microscopy. *Opt. Lett. Vol. 42, Issue 7, pp. 1269-1272* **42**, 1269–1272 (2017).

9. Hirvonen, L. M. *et al.* Lightsheet fluorescence lifetime imaging microscopy with wide-field time-correlated single photon counting. *J. Biophotonics* **13**, e201960099 (2020).

10. Nutt, K. J. *et al.* High-efficiency digitally scanned light-sheet fluorescence lifetime microscopy (DSLM-FLIM). *bioRxiv* 2023.06.02.543377 (2023). doi:10.1101/2023.06.02.543377

11. Samimi, K. *et al.* Light-sheet autofluorescence lifetime imaging with a single-photon avalanche diode array. *https://doi.org/10.1117/1.JBO.28.6.066502* **28**, 066502 (2023).

12. Bowman, A. J., Huang, C., Schnitzer, M. J. & Kasevich, M. A. Wide-field fluorescence lifetime imaging of neuron spiking and subthreshold activity in vivo. *Science.* **380**, 1270–1275 (2023).

13. Bowman, A. J., Klopfer, B. B., Juffmann, T. & Kasevich, M. A. Electro-optic imaging enables efficient wide-field fluorescence lifetime microscopy. *Nat. Commun. 2019 101*

10, 1–8 (2019).

14. Galland, R. *et al.* 3D high-and super-resolution imaging using single-objective SPIM. *Nat. Methods* **12**, 641–644 (2015).

15. Singh, A. P. *et al.* 3D Protein Dynamics in the Cell Nucleus. *Biophys. J.* **112**, 133–142 (2017).

16. Beghin, A. *et al.* Automated high-speed 3D imaging of organoid cultures with multi-scale phenotypic quantification. *Nat. Methods 2022* 1–12 (2022). doi:10.1038/s41592-022-01508-0

17. PicoQuant GmbH. High-power picosecond pulses at 488 nm. Available at: https://www.picoquant.com/scientific/product-studies/high-power-picosecond-pulses-at-488-nm. (Accessed: 18th March 2024)

18. Loidolt-Krüger, M. *et al.* Visualize dynamic processes with rapidFLIMHiRes, the ultra fast FLIM imaging method with outstanding 10 ps time resolution. Available at: https://www.picoquant.com/dl_technotes/AppNote_rapidFLIM_HiRes.pdf. (Accessed: 19th March 2024)

19. Antolovic, I. M., Burri, S., Bruschini, C., Hoebe, R. & Charbon, E. Nonuniformity analysis of a 65-kpixel CMOS SPAD imager. *IEEE Trans. Electron Devices* **63**, 57–64 (2016).

20. Tomer, R., Khairy, K., Amat, F. & Keller, P. J. Quantitative high-speed imaging of entire developing embryos with simultaneous multiview light-sheet microscopy. *Nature Methods* **9**, 755–763 (2012).

21. Krzic, U., Gunther, S., Saunders, T. E., Streichan, S. J. & Hufnagel, L. Multiview light-sheet microscope for rapid in toto imaging. *Nat. Methods* **9**, 730–733 (2012).

22. Scipioni, L., Rossetta, A., Tedeschi, G. & Gratton, E. Phasor S-FLIM: a new paradigm for fast and robust spectral fluorescence lifetime imaging. *Nat. Methods 2021 185* **18**, 542–550 (2021).

23. Digman, M. A., Caiolfa, V. R., Zamai, M. & Gratton, E. The phasor approach to fluorescence lifetime imaging analysis. *Biophys. J.* **94**, L14–L16 (2008).

24. Fereidouni, F., Esposito, A., Blab, G. A. & Gerritsen, H. C. A modified phasor approach for analyzing time-gated fluorescence lifetime images. *J. Microsc.* **244**, 248–258 (2011).

25. Ragaller, F. *et al.* Quantifying Fluorescence Lifetime Responsiveness of Environment-Sensitive Probes for Membrane Fluidity Measurements. *J. Phys. Chem. B* **128**, 50 (2023).

26. Royer, C. *et al.* ASPP2 maintains the integrity of mechanically stressed pseudostratified epithelia during morphogenesis. *Nat. Commun. 2022 131* **13**, 1–19 (2022).

27. Roffay, C. *et al.* Technical insights into fluorescence lifetime microscopy of mechanosensitive Flipper probes. *bioRxiv* 2022.09.28.509885 (2023).

doi:10.1101/2022.09.28.509885

28. Wahl, M. *et al.* Photon arrival time tagging with many channels, sub-nanosecond deadtime, very high throughput, and fiber optic remote synchronization. *Rev. Sci. Instrum.* **91**, (2020).

29. Pi Imaging. SPAD512^2 system manual. Available at: https://piimaging.com/doc-spad512s. (Accessed: 18th March 2024)

30. Zewail, S. P. A. H. Femtosecond real time probing of reactions XXII Kinetic description of probe absorption fluorescence depletion and mass spectrometry. *Mol. Phys.* **89**, 1455–1502 (1996).

31. Ourselin, S., Roche, A., Prima, S. & Ayache, N. Block matching: A general framework to improve robustness of rigid registration of medical images. *Lect. Notes Comput. Sci. (including Subser. Lect. Notes Artif. Intell. Lect. Notes Bioinformatics)* **1935**, 557–566 (2000).

32. Medeiros, G. De *et al.* Confocal multiview light-sheet microscopy. *Nat. Commun.* **6**, (2015).

33. Guignard, L. *et al.* Contact area-dependent cell communication and the morphological invariance of ascidian embryogenesis. *Science.* **369**, (2020).

34. Aigouy, B., Umetsu, D. & Eaton, S. Segmentation and Quantitative Analysis of Epithelial Tissues. *Methods Mol. Biol.* **1478**, 227–239 (2016).

35. Schindelin, J. *et al.* Fiji: an open-source platform for biological-image analysis. *Nat. Methods* **9**, 676–682 (2012).

36. Ahlers, J. *et al.* napari: a multi-dimensional image viewer for Python. (2023). doi:10.5281/zenodo.8115575

37. Baillie-Johnson, P., van den Brink, S. C., Balayo, T., Turner, D. A. & Arias, A. M. Generation of Aggregates of Mouse Embryonic Stem Cells that Show Symmetry Breaking, Polarization and Emergent Collective Behaviour In Vitro. *JoVE (Journal Vis. Exp.* **2015**, e53252 (2015).

38. Hashmi, A. *et al.* Cell-state transitions and collective cell movement generate an endoderm-like region in gastruloids. *Elife* **11**, (2022).